Available online at www.sciencedirect.com

Journal of Applied Research and Technology

Journal of Applied Research and Technology 13 (2015) 566–575

www.jart.ccadet.unam.mx

Original

Fabrication and photophysical studies of CdTe quantum-dots dispersed in SiO_2 sonogel optical-glasses

Omar G. Morales-Saavedra [a,*], Claudio D. Gutiérrez-Lazos [b], Mauricio Ortega-López [c], Antonio A. Rodriguez-Rosales [a]

[a] *Centro de Ciencias Aplicadas y Desarrollo Tecnológico, Universidad Nacional Autónoma de México, Circuito Exterior S/N, Ciudad Universitaria, Apartado Postal 70-186, México D.F. 04510, Mexico*

[b] *Facultad de Ciencias Físico-Matemáticas, Universidad Autónoma de Nuevo León, 66451 San Nicolás de los Garza, NL, Mexico*

[c] *Departamento de Ingeniería Eléctrica, Sección de Electrónica del Estado Sólido, Centro de Investigación y de Estudios Avanzados del Instituto Politécnico Nacional, Av. Instituto Politécnico Nacional 2508, Col. San Pedro Zacatenco, 07360 México D.F., Mexico*

Received 21 April 2015; accepted 22 September 2015

Available online 28 November 2015

Abstract

The catalyst-free sonogel route has been implemented to fabricate highly pure SiO_2 glasses as host materials for CdTe quantum dot nanocrystals synthesized in aqueous solution. Developed CdTe-based inorganic–inorganic hybrid composites exhibited rigid bulk structures with controllable geometrical shapes and dopant concentrations, allowing the control of the optical properties in the solid-state confinement. Comprehensive linear and nonlinear photophysical characterizations were performed according to UV–vis absorbance, Raman and photoluminescent spectroscopies; the linear refractive indices of highly/lowly CdTe-doped samples were also estimated according to the Brewster angle technique. Since the hybrid glasses are amorphous in nature, the cubic nonlinear optical activity of these composites has been tested via the Z-Scan technique. Results show that the CdTe quantum dots were homogeneously embedded within the SiO_2-sonogel matrix with only small guest–host molecular interactions and preserving their strong photoluminescent properties; thus providing advanced solid-state heterostructured nanocomposite materials suitable for current technological photonic applications.

Keywords: Cadmium telluride; Quantum dot; Spectroscopy; Nonlinear optics; Hybrid material; Sol–gel

1. Introduction

Inorganic semiconductor nanocrystals (NCs) or quantum dots (QDs) exhibit physical and chemical properties which considerably differ from their individual molecules or bulk forms, due to quantum confinement effects (Kagan, Murray, & Bawendi, 1996; Rogach et al., 2007). These properties have a huge interest for applications in optoelectronics (Gao et al., 2000; Hollingsworth et al., 2001; Schlamp, Peng, & Alivisatos, 1997), photovoltaic devices (Huang, De Valle, Kana, Simmons-Potter, & Potter, 2015; Rajbanshi, Sarkar, & Sarkar, 2014; Sehgal & Narula, 2015), optical amplifier media for telecommunication networks (Harrison et al., 2000), and biolabeling/biomedical devices (Chao, Hu, & Chen, 2014; Gao, Cui, Levenson, Chung, & Nie, 2004). A relatively recent approach to realize electroluminescent devices has emerged from the development of colloidal quantum dots, because they can be synthesized in organic solvents (Murray, Norris, & Bawendi, 1993) or water (Gaponik et al., 2002a; Gaponik, Talapin, Rogach, Eychmüller, & Weller, 2002b). Besides, the nanocrystals surface can be conveniently functionalized to transfer it from water to an organic solvent (Gaponik et al., 2002a, 2002b) or vice versa, depending if a given application requires the use of polar or apolar solvents. The nanocrystals physicochemical properties strongly depend on the surface characteristics as the nanoparticle size is reduced below the Bohr exciton diameter; this is due to its very high surface/volume ratio. Therefore, the nanocrystals surface must be functionalized in order to activate the optical properties; for instance, luminescence. In a colloidal solution, nanocrystals are protected against aggregation by an organic capping layer

* Corresponding author.
E-mail address: omar.morales@ccadet.unam.mx (O.G. Morales-Saavedra).
Peer Review under the responsibility of Universidad Nacional Autónoma de México.

http://dx.doi.org/10.1016/j.jart.2015.10.013

formed by surfactant monomers. These compounds interact with the nanocrystals surface to passivate the surface sites, minimizing the non-radiative recombination. The color of emission can be tuned by varying the nanocrystals size, whereas narrowing the size distribution allows for photoluminescence peaks with FWHM (full width at half maximum) of only 20–30 nm (Talapin, Rogach, Kornowski, Haase, & Weller, 2001). It has been demonstrated by several research groups that nanosized II-VI semiconductors can be used as emitting materials in thin film electroluminescence devices (Ando, Hosokawa, Yang, & Murase, 2012; Li, Liu, Xie, & Liu, 2013; Tu, Su, & Chen, 2014).

Indeed, in the last decade semiconductor QDs systems have been intensively studied from the fundamental point of view in physics and chemistry due to their potential applications in photonics (Chu et al., 2012; Kostić & Stojanović, 2012; Zhao, Sun, Wang, Du, & Wang, 2012). However, most of these studies have been traditionally performed in powder samples, colloidal suspensions or in thin film formats. Under this perspective, we investigate in this work on the optical properties of CdTe-QDs nanocrystals immersed in SiO_2 glassy networks grown via the sonogel route (Flores-Flores & Saniger, 2006; Morales-Saavedra et al., 2007; Torres-Zúñiga & Morales-Saavedra, 2012). Because of the high specific surface areas, uniform nanopore size distribution and appropriate chemical stability, mesoporous sol–gel materials have been recently used as hosting networks for metal and metal oxide nanoparticles (MNPs) which promise potential applications in many technologically important areas (Morales-Saavedra et al., 2012). Apparently, the use of mesoporous oxide structures with high specific surface areas as hosting systems for MNPs can dramatically improve their functionalities such as magnetic, catalytic and optoelectronic activities. The main advantages here are the low manufacturing costs involved in the fabrication process of these kinds of advanced heterostructures, a straightforward room temperature (RT) material processing, and an easy sample malleability/manipulation attainable during/after the fabrication-stage, respectively. Under this framework, it is worth performing photophysical studies with semiconductor CdTe-QDs systems immersed in SiO_2 sol–gel networks. In fact, since SiO_2 is optically transparent over a wide spectral range and is electrically insulating, it can serve as an excellent medium for embedding such semiconductor nanostructures; bringing high affinity and a neutral environment for the inclusion of these systems. The resulting solid-state hybrid structures may also exhibit practical and low-cost alternatives for the development of bulk samples with high QDs dopant content and malleable shape/size within a highly pure/inert SiO_2 environment. This provides a simple way to study the photophysical properties of these QDs/NCs in a quasi-pristine form and in a desired sample format.

2. Materials and methods

2.1. Synthesis of CdTe-QDs

2.1.1. Reagents

Cadmium chloride hydrate ($CdCl_2xH_2O$, 99% Johnson-Matthey), sodium borohydride ($NaBH_4$, ~98% Sigma–Aldrich), tellurium powder (−200 mesh, 99.8% Aldrich), thioglycolic acid (TGA, ≥98.0% Fluka) and Poly(diallyldimethylammonium chloride) (PDDA, Mw: 100,000–200,000, 20 wt% in water, Aldrich).

2.1.2. CdTe-QDs synthesis

The CdTe nanocrystals were prepared from aqueous solutions of NaHTe and Cd_2+ (Gaponik et al., 2002a, 2002b). The telluride ion precursor was prepared according to reference (Gu, Zou, Fang, Zhu, & Zhong, 2008; Gutiérrez-Lazos et al., 2010) under N_2 atmosphere. The Cd_2+ precursor was prepared by mixing $CdCl_2$ and TGA as stabilizer in deionized water, maintaining the Cd/TGA molar ratio and pH at 1:6 and 5, respectively; the pH being adjusted with 3 M NaOH aqueous solution. The Cd/Te molar ratio was 4:1. In the synthesis process, the Cd_2+ and NaHTe were thoroughly mixed at room temperature and under N_2 flow. The mixture was then heated up to 92 °C under open-air conditions in an erlenmeyer flask for different heating times. Two samples (sample A: 3 h; sample B: 1 h, according to the present study) were taken at different growth times and tested for UV–vis absorbance and photoluminescence (PL) measurements. Under this methodology, the mean CdTe-QDs nanocrystals size obtained for samples A and B were 2.6 nm and 2.2 nm, respectively.

2.2. Synthesis of SiO_2-based sonogels

2.2.1. Reagents

Tetraethyl-orthosilicate (TEOS, Fluka 99% purity) and tridistilled water (SIGMA).

2.2.2. SiO_2-sonogel synthesis

In this work, a different approach from the traditional sol–gel process is implemented for the preparation of highly pure SiO_2-based sonogel materials. Here, the use of both solvents and catalysts is fully suppressed and the hydrolyzed species are substituted by molecular radicals generated by ultrasound. Extensive details on this methodology to produce catalyst-free sonogel materials have been given in the literature (Flores-Flores & Saniger, 2006; Morales-Saavedra et al., 2007; Torres-Zúñiga & Morales-Saavedra, 2012). According to this procedure, a precursor solution of 25 mL of TEOS and 25 mL of tridistilled/neutral water were mixed into a glass vessel and stabilized at 1 °C for 1 h before ultrasonic (US) irradiation within a thermal bath used as cooling system (these reactants are non-soluble). An ultrasound tip (Cole-Parmer-CPX, 1.25 cm in diameter), located at the TEOS/H_2O surface interface provides an effective irradiation power density on the order of ~3.2 W cm^{-3} (@ 20 kHz). After 3 h of programmed US-irradiation (on/off-intermittent sequences of 5 s; net irradiation time: 1.5 h), the TEOS/H_2O temperature mixture was increased up to ~6 °C due to the energetic US-waves provided to the reactants; afterwards the cooling system was turned off and the sonicated suspension was kept in the reactor vessel at room conditions for 24 h. Thereafter, two immiscible and highly transparent liquid phases appear: the upper one, corresponding to unreacted TEOS was removed, whereas the lower and more dense phase,

corresponding to a stable colloidal suspension and containing the ultrasonically induced hydrolyzed product (OH-TEOS) is capable of producing (after drying-condensation and polymerization processes) a highly pure SiO_2 glassy network. In order to fabricate sonogel hybrid materials, the CdTe-QDs doping procedure must be performed in the liquid sol-phase. Hence, the CdTe-QDs/H_2O dopant sample (in deionized water), as obtained from the synthetic route described above, can directly be used. The CdTe-QDs based solutions (samples A and B) are respectively added and ultrasonically mixed to the OH-TEOS colloid in order to structure homogeneous doped mixtures; these mixtures are then ready to be used for spin-coating and/or shape-designed mold deposition procedures (bulk samples). For bulk monolith hybrid sample preparation, the dose ratio of the OH-TEOS versus the dopant-solution (OH-TEOS:DS) was prepared with a precise volumetric micropipette and deposited into cylindrical Teflon-molds (1 in. in diameter, 2 mL in volume) in order to obtain different lightly/heavily loaded sonogel (SG) hybrid glasses. SG-samples at high/low dopant concentrations were prepared according to this methodology with a starting volume of 2 mL by varying the (OH-TEOS:DS) concentration ratio (in volume) as follows: (1.0:1.0), (1.5:0.5), (1.6:0.4), (1.8:0.2) and (1.9:0.1) mL. Undoped/pure reference sonogel samples (PR-SG) at (2.0:0.0) were also prepared for reference and spectroscopic calibration purposes. The samples were isolated while drying with a plastic box in order to avoid atmosphere and temperature variations, and conserved for ~30 days at room conditions in closed recipients with a small hole in the cap within a clean-dry-dark environment. Rigid and geometrical hybrid monoliths, adequate for optical applications were obtained after this slow drying process. The resulting hybrid glasses possess higher chemical purity compared to other traditional synthesized sol–gel doped composites due to the use of US-waves instead of reactive solvents/catalyst.

2.3. Instrumentation and characterization techniques

Standard spectroscopic material characterization techniques were applied to the obtained hybrid samples: (a) UV–vis absorbance spectroscopy: a Double beam Shimadzu-260 spectrophotometer and a Edmond CCD/BRC112E/EO UV–Vis spectrometer were implemented for high resolution transmittance measurements; (b) Raman spectroscopy: Almega-XR Dispersive Micro-Raman spectrometer (Olympus 50X objective lens; optical excitation source: a frequency-doubled Nd:YVO_4 laser system @ 532 nm, 8 mW); (c) linear photoluminescent (PL) measurements (FluoroMax-3, Jobin-Yvon-Horiba fluorimeter). The excitation wavelength was selected according to the UV–vis absorbance spectra (near to λ_{max}); (d) the evaluation of the linear refractive index n_B of the hybrid glasses was carried out with an unpolarized He–Ne Laser system ($\lambda = 632.8$ nm) and a linear polarizer, following the Brewster-angle methodology (Eugene, 2002); (e) finally, the obtained hybrid glasses were also studied as active media for cubic $\chi^{(3)}$ nonlinear optical (NLO) effects via the Z-Scan technique. The Z-Scan experimental set-up was implemented using an unpolarized He–Ne laser system (THORLABS, HRR170-1 @ $\lambda = 632.8$ nm, 35 mW) (Rodríguez-Rosales, Morales-Saavedra, Román-Moreno, & Ortega-Martínez, 2008). The spatial mode of the laser beam was close to Gaussian TEM_{00}. The polarization plane of the laser was controlled by means of a linear polarizer mounted on a rotation stage. The laser beam was focused on the sample via a positive lens ($f = 5$ cm), so that the light power density at the focal spot on the sample was about 8.53×10^6 W m^{-2}. Samples were mounted on a motorized translation stage (25 mm length travel in steps of 2 μm) in order to perform Z-Scan experiments. A large area Si-photodetector (EOT ET-2040) was located at ~0.96 m from the focusing lens, after a 2.5 mm diameter (~20% transmittance) diaphragm-aperture. NLO-signals captured from photo-detectors were measured with a digital oscilloscope (Tektronix TDS, 744A) and the experimental set-up administration was performed via a Lab-View Master-program and the corresponding device drivers.

3. Results and discussions

3.1. Fabrication process of the CdTe-QDs/SiO_2 hybrid sonogels and linear refractive index measurements

In Figure 1 typical results of the sonogel fabrication process is illustrated. Here, the initially filled Teflon containers (1 in. in diameter) exemplify, after several days, the shrinking sequence of the hybrid glasses due to sample dehydration. The characteristic green-yellow color of the CdTe-QDs can be observed from the beginning of the sample preparation phase, becoming more intense as the doped samples become denser due to the sol drying course. The intense and homogeneous color achieved after drying, confirms the correct and regular dispersion of the CdTe-QDs within the glassy sonogel networks. It has been observed that CdTe-QDs based hybrid samples are less susceptible to fractures if purity and environment conditions are favorable. Indeed, after a few weeks of aging, once the drying course is optimally accomplished, rigid hybrid monoliths with controllable geometrical shapes can be obtained (with 70–90% efficiency for slightly and heavily doped samples, respectively): this gives rise to bulk samples with controllable QDs molecular loading and desired structures. The faces of the hybrid glasses (exposed to air while drying) exhibit a fairly flat surface with a high-gloss mirror-finish which is highly adequate for overall optical and spectroscopic studies. These quasi-polished samples, as obtained after drying, generally exhibit good optical surface quality, making these samples suitable for overall photophysical characterizations.

The estimated values of the linear refractive index n_B of several CdTe-QDs hybrid glasses prepared at different dopant concentrations are shown in Table 1. In general, the refractive index of CdTe-QDs in aqueous solutions is in the order of 1.335–1.380, depending on the preparation conditions (Chen et al., 2008). In our case however, the refractive index of the bulk hybrid sonogels (HSG) is larger due to the solid-state confinement and higher molecular packing promoted by this phase. From Table 1, it is also observed that the n_B-values of the hybrid composites are larger than that measured for an undoped/pure reference glass: PR-SG @ (2.0:0.0). The latter fact is due to the

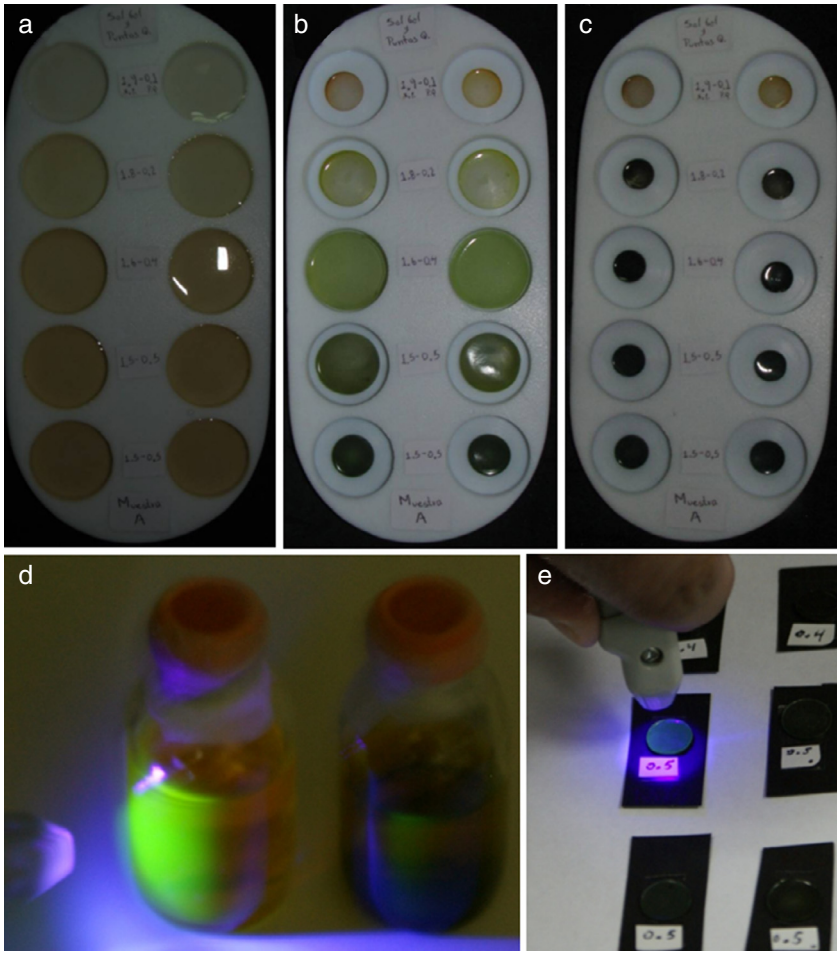

Fig. 1. Fabrication process of a heavily/lowly CdTe-QDs doped sonogel hybrid glasses: (a) Teflon molds filled-up with a mixture of CdTe-QDs/H_2O and the OH-TEOS product (in sol phase); (b) after few days of aging, the drying process reduces the size of the forming hybrid monoliths (the shrinking rate depends on the OH-TEOS:DS ratio); (c) after 3–4 weeks, the drying course is finished; this slow dehydration process stimulates optimal polymerization of the SiO_2 network, giving rise to rigid glassy monoliths with controllable/designed geometrical shapes and homogeneous dopant distributions; (d) photograph of the starting green-yellow colored CdTe-QDs aqueous solutions (samples A and B) excited with an UV/Violet light source: the strong green fluorescence, typical of these materials can be easily recognized; (e) hybrid CdTe-QDs/SiO_2 sonogel glasses excited with the UV/Violet source: in this case a blue-green fluorescence arise from the opaque (highly loaded) HSG-composites.

Table 1
Linear refractive index values (n_B) of the developed CdTe-QDs/SiO_2-based sonogel hybrid composites at different dopant concentrations (sample A). Measurements were performed according to the Brewster angle methodology ($\lambda_{EX} = 632.8$ nm).

Hybrid sonogel (HSG), CdTe-QDs/H_2O & PR-SG samples	Linear refractive index values: n_B (± 0.02)
Pure Reference Sonogel PR-SG @ (2.0:0.0)	1.33
Pristine CdTe-QDs/H_2O	1.35
HSG @ (1.9:0.1)	1.38
HSG @ (1.8:0.2)	1.40
HSG @ (1.6:0.4)	1.43
HSG @ (1.5:0.5)	1.46
HSG @ (1.0:1.0)	1.49

inherent high porosity of the SG-matrix. Indeed, the PR-SG network exhibits the lower n_B-value given the high surface area of its internal nanopores; these cavities mainly contain air inside, as most of the solvent/water residuals evaporate during the long shrinking/drying course. Hence, the refractive index of a PR-SG sample approaches unity. In contrast, for hybrid SG-systems, the CdTe-QDs guest nanocrystals fill-up a vast number of cavities during the drying course, increasing the respective HSG linear refractive indices according to the selected dopant-loading and allowing the tuning of the optical properties.

3.2. Optical absorbance and photoluminescence (PL) spectroscopic inspections

Absorbance/Transmittance and PL-spectroscopic measurements were initially carried out in order to provide preliminary information concerning the electronic properties of the hybrid materials for linear and NLO-applications, to test the optical quality of the samples and to verify the correct inclusion of the semiconducting CdTe-QDs guests within the porous SiO_2-sonogel network. Absorbance/Transmittance and PL-spectra of the CdTe-QDs were obtained in both aqueous solutions and in the solid-state HSG-phase. The corresponding absorbance

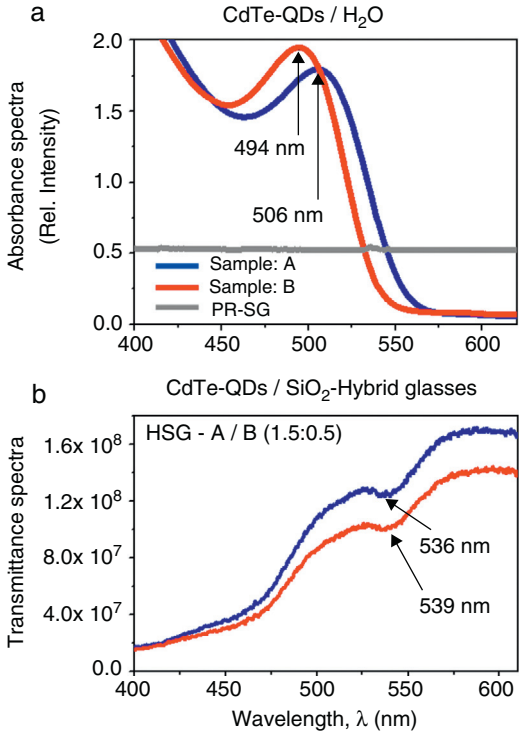

Fig. 2. (a) Comparative absorbance spectra of the CdTe-QDs systems in aqueous solutions (samples A–B) and the (2.0:0.0) reference/pure sonogel matrix (PR-SG); (b) comparative high-resolution transmittance spectra of the CdTe-QDs/SiO_2-based hybrid sonogel composites [HSG-glasses of samples A and B @ (1.5:0.5) doping rate].

spectra are shown in Figure 2a and b. The absorbance spectra of the starting CdTe-QDs/H_2O (Figure 2a) present broad and well defined bands around 500 nm; the sample with larger crystallite size (sample A) exhibit a smaller absorbance peak at 506 nm and a redshift in its maximum with respect to the absorbance peak of sample B (located at 494 nm), which is consistent with the preparation reaction time increase for aqueous samples (Gutiérrez-Lazos et al., 2010). Indeed, this red shift is usually observed in semiconductor nanocrystals and it has been attributed to the crystallite size increase (Brus, 1984). Interestingly, the emission spectra of the studied samples display peaks with FWHM ranging from 40 to 50 nm, indicating a relatively narrow size distribution for the studied CdTe-QDs, which compares well with that reported for CdTe colloids synthesized by organometallic and colloidal methods (Gaponik et al., 2002a, 2002b).

On the other hand, the (2.0:0.0) reference sonogel glass shows comparatively small absorption in the visible region due to its intrinsic high purity level, and an increasing absorption to the UV-region which is typical of SiO_2-glassy materials (UV-region not shown in Figure 2a). These facts indicate optimal conditions for the observance of the molecular electronic spectra of the CdTe-QDs embedded within the SG-glasses. However, as shown in Figure 1, due to the opacity of the HSG samples, high resolution transmittance measurements were performed in order to elucidate the main spectroscopic features of these composites. In fact, Figure 2b reveals low transmittance regions within the 530–540 nm spectral range; these well-defined valleys/minima in the transmittance spectra correspond to the absorbance bands of the QDs within the HSG environment. However, a larger red shift of ~35 nm occurs in these bands (valleys) for the hybrid samples with respect to the absorbance features of the starting aqueous samples. The observation of these bands (transmittance minima) evidences the convenient CdTe-QDs loading within the porous SG-network, although a NC size increase is evident due to the higher QDs-concentration promoted by a dense molecular packing within this solid-state confinement. This provokes a lower resolution of the absorption bands due to bulk-like material behavior. However, because of the relatively weak interaction between silica and the CdTe-QDs, mesoporous silica is able to effectively reduce the NC QDs mobility and their tendency toward coarsening at operative room conditions. Indeed, the chemically inactive mesoporous SiO_2 support often does not participate in any undesired reaction which may frustrate several designed applications for the original NC CdTe-QDs nanostructures; thus preserving as high as possible their pristine properties, as it is shown below.

It is worthy to note that the absorptive properties of the hybrid composites at the laser frequency implemented for linear and nonlinear refractive measurements ($\lambda = 632.8$ nm) are reasonably far from resonant conditions. This means that the strongest absorption effects occurring around ~540 nm may be reasonably ignored in NLO/Z-Scan-experiments, as will be discussed in more detail in Section 3.3. In the present case, it can be considered that the Z-Scan experiments may be recorded in reasonably off-resonant conditions.

Figure 3a and b illustrates the comparative PL-spectra of the CdTe-QDs aqueous-solutions (samples A and B). The emission experiments evidence a remarkable increase of the luminescent properties as the excitation wavelength increase. In fact, according to the absorbance spectra, optimal excitation is achieved at a wavelength near the absorption maxima of each sample. For sample A, the highest PL-activity is achieved at an excitation wavelength of $\lambda_{EX} = 508$ nm, with a strong green emission at $\lambda = 556$ nm whereas for sample B, the highest PL-activity can be observed at $\lambda_{EX} = 495$ nm, also showing a strong green emission at $\lambda = 540$ nm. According to these results excitation experiments were carried out in order to investigate in more detail the PL-features of these samples at best emission wavelengths in each case. Accordingly, the inset graphs in Figure 3a and b exhibit the excitation experiments performed in samples A and B as these solutions were inspected at their optimal emission wavelengths ($\lambda_{EM} = 556$ nm and $\lambda_{EM} = 540$ nm, respectively). It is clear from these experiments that most favorable optical excitations can be performed within the green range (520–560 nm) in order to produce strong green PL-activity in both samples, although excitation within the violet-blue range (400–500 nm) may also produce significant green PL-emissions. The PL-emission intensities of both samples are very similar, being this activity larger for sample A.

Figure 4a and b shows the comparative PL-spectra of the CdTe-QDs/SiO_2 sonogel hybrid glasses (given the similarities between the HSG samples A and B, we only show the results for sample A at three different dopant concentrations).

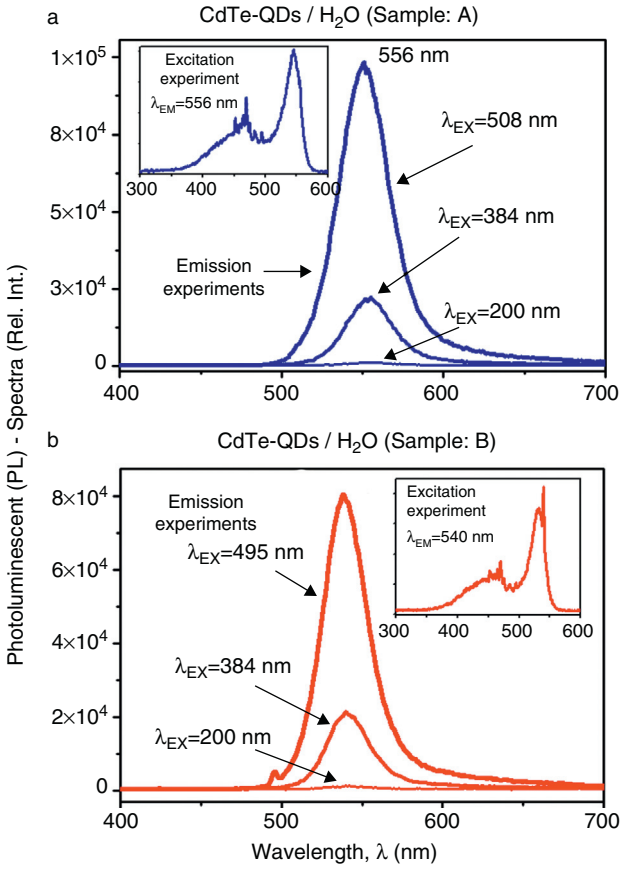

Fig. 3. Comparative PL-spectra of the CdTe-QDs systems in aqueous solutions (samples A–B): (a) PL-spectra of sample A recorded in emission experiments at different excitation wavelengths. Inset figure: excitation experiment recorded at the emission wavelength of $\lambda_{EM} = 556$ nm; (b) PL-spectra of sample B recorded in emission experiments at different excitation wavelengths. Inset figure: excitation experiment recorded at the emission wavelength of $\lambda_{EM} = 540$ nm.

Again, the emission experiments evidence an important PL-intensity increase as the excitation wavelength augments from $\lambda_{EX} = 200$ nm to $\lambda_{EX} = 425$ nm, where optimal PL-emissions at 470 nm can be observed. In this case however, the excitation wavelengths do not correspond to the respective absorbance bands of the HSG-composites and the appearance of strong violet-blue PL-signals with excitation energies compared to those used in the aqueous samples points to a complex quantum electronic structure of the CdTe-QDs/SiO_2-hybrid systems with possible overlapping quantum states, multiphoton absorption/excitation processes and energy transfer properties. These effects should have a direct impact on the NLO-properties of these solid-state samples as will be discussed in the next section. Besides, as the slightly/heavily doped HSG-samples are excited at $\lambda_{EX} = 425$ nm, two major and more intense PL-bands, with narrower bandwidths come out, namely at 383 and 470 nm. Given that the main blue emission peak observed at 470 nm appears at both excitation wavelengths ($\lambda_{EX} = 200$ and 425 nm), the inset graph in Figure 4b shows the excitation experiment performed in a lowly doped (1.8:0.2) SG sample (at $\lambda_{EM} = 470$ nm). Here, the importance of this blue emission peak (at 470 nm) becomes evident as the sample is exited within the green region (at $\lambda_{EX} \approx 515$ nm). This confirms, as explained before, the

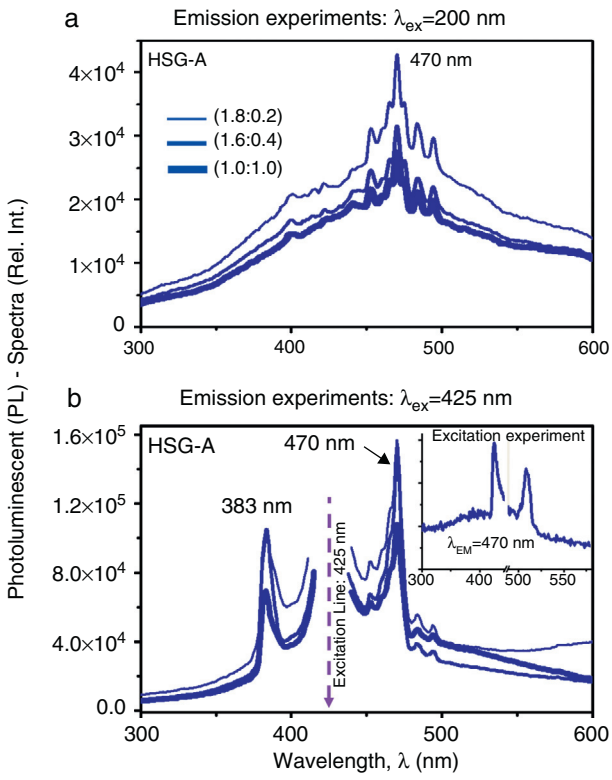

Fig. 4. Comparative PL-spectra of the CdTe-QDs/SiO_2 hybrid sonogel glasses (sample A) at different dopant concentrations: (a) PL-spectra of the HSG-glasses recorded in emission experiments at $\lambda_{EX} = 200$ nm. (b) PL-spectra of the HSG-glasses recorded in emission experiments at $\lambda_{EX} = 425$ nm. Inset figure: excitation experiment recorded in a (1.8:0.2) doped composite at $\lambda_{EM} = 470$ nm.

dominant violet-blue emission process within the CdTe-QDs/SiO_2 sonogel hybrid composites.[1]

According to the emission experiments shown in Figure 4a and b, the PL-intensities of the hybrid glasses are, in general, an order of magnitude higher than their aqueous counterparts at similar excitation wavelengths. It is also observed that the PL-intensity of the HSG-samples show a dependence with the CdTe-QDs dopant concentration. In fact, as the doping rate augments from the slightly doped (1.8:0.2) HSG-sample to the heavily doped (1.0:1.0) one, the PL-emissions tend to decrease. This behavior can be understood by considering the opacity of the hybrid glasses and the corresponding self-absorption effects; indeed, for higher dopant concentrations, the optical density of the HSG-glasses increases due to the higher CdTe-QDs NC-concentration. This densely packed matter state produces high PL-activity but also strong self-absorption effects due to the high molecular packing[2]; thus quenching the PL-emissions of the HSG-sample. Conversely, for slightly doped HSG-glasses, the PL-activity of the QDs-NCs within the volume of the

[1] Intense blue-shifted excitonic emission peaks with increased luminescence have been also observed in CdTe-QDs thin films with increasing number of layers. However, a full explanation of this phenomenon has not yet been given (Gutiérrez-Lazos et al., 2010).

[2] The formation of densely packed CdTe-QDs structures/aggregates within the solid-state SG-network could also promote the nucleation of larger CdTe crystals with a bulk-like behavior and worse PL-activity.

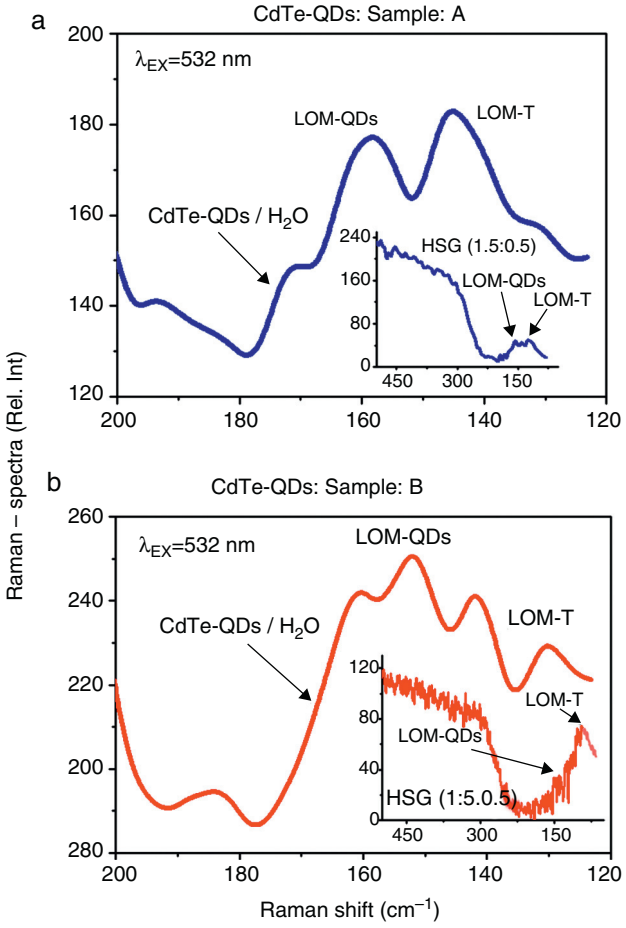

Fig. 5. Comparative Raman emission spectra of the CdTe-QDs immersed in both H_2O-aqueous solutions and SiO_2-HSG environments: (a) Raman signals obtained from sample A in aqueous solutions. Inset figure: Raman signals obtained from the respective HSG-glass at (1.5:0.5) doping rate. (b) Raman signals obtained from sample B in aqueous solutions. Inset figure: Raman signals obtained from the respective HSG-glass at (1.5:0.5) doping rate. Raman experiments were carried out at $\lambda_{EX} = 532$ nm. The typical low-modes for low-dimensional CdTe-QDs nanocrystals can be recognized in both kinds of samples and environments.

HSG-glasses can be easily registered. It is clear that the strong absorptive properties of these solid-state samples can also affect the NLO-properties of the HSG-systems, as discussed in the next section.

3.3. Raman and Cubic NLO/Z-Scan spectroscopic inspections

The Raman spectroscopic measurements performed in both aqueous solutions and the HSG environments are shown in Figure 5a and b. An overlap of several low-modes (LOM) within the 120–180 cm^{-1} wave-number interval can be easily recognized in the Raman emissions obtained from the CdTe-QDs/H_2O and CdTe-QDs/SiO_2 (A–B) samples. These LOM-modes are typical for low dimensional CdTe particles and evidence the fact that the CdTe-QDs nanocrystals, initially synthesized in aqueous solution, have been successful assembled within the SiO_2 sonogel environment (at least at moderate-to-high percentage,

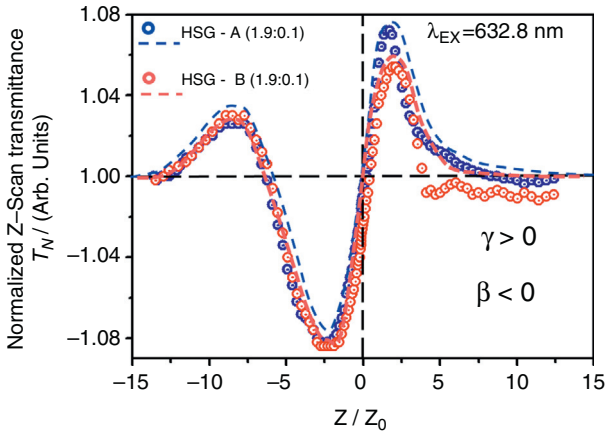

Fig. 6. Closed aperture Z-Scan measurements (normalized transmittance: T_N) obtained from the CdTe-QDs/SiO_2-based HSG-composites at different QDs sizes (samples A and B). Slightly (1.9:0.1) doped glasses were selected for this study in order to obtain best possible NLO/Z-Scan signals from the pristine CdTe-QDs nanocrystals within the immersing SG-phase. Open circles: experimental results; dashed lines: theoretical fits (TF).

allowing the luminescent Raman detection). Here, the Raman peaks located within the 130–145 cm^{-1} range can be assigned to CdTe tetrapods (LOM-T); whereas the Raman emissions detected within the 150–165 cm^{-1} interval can be precisely correlated to the LO modes of CdTe quantum dots (Gutiérrez-Lazos et al., 2010; De Paula et al., 1996). These LOM-Raman peaks can be only observed from slightly doped HSG-samples: from (1.5:0.5) to (1.9:0.1) dopant concentrations. For heavily doped HSG-composites: (1.4:0.6) to (1.0:1.0) dopant concentrations (not shown here for simplicity in the graphs), the Raman peaks tend to disappear and only a weak envelope signal takes place within the 120–180 cm^{-1} wave-number interval; this suggests the formation of massive CdTe-aggregates and the appearance of LOM for bulk CdTe at such dopant concentrations (highly loaded HSG-glasses).

Finally, according to the latter observations, we have performed Z-Scan measurements in slightly doped HSG-composites in order to test the cubic $\chi^{(3)}$-nonlinear refractive optical response of these samples. In this way, we can assure that the lowly doped HSG-lasses will elucidate the main NLO-properties of the CdTe-QDs embedded within the solid-state sonogel confinement. According to Figure 6, the NLO/Z-Scan measurements obtained from both samples are quite similar (in shape); being the curve corresponding to sample A slightly larger in its normalized transmittance (if the absolute value of the main valley-to-peak distance is considered). Taking into account the theory developed for Z-Scan experiments (Liu, Guo, Wang, & Hou, 2001; Sheik-Bahae, Said, & Van Stryland, 1989; Sheik-Bahae, Said, Wei, Hagan, & Van Stryland, 1990), it is observed from our experimental results that the nonlinear refractive response of the studied samples can be unambiguously determined by typical valley-to-peak Z-Scan transmittance curves (closed aperture mode). Consequently, one can immediately state that the CdTe-QDs/SiO_2-based HSG-composites exhibit a dominant positive NLO-refraction coefficients (γ or $n_2 > 0$)

for both implemented CdTe-QDs sizes, satisfying the following relation:

$$|\gamma(\mathrm{CdTe^A} - \mathrm{QDs/SiO_2})| > |\gamma(\mathrm{CdTe^B} - \mathrm{QDs/SiO_2})|$$

On the other hand, a flat Z-Scan curve was obtained from the highly transparent undoped PR-SG sample (not shown here for simplicity), indicating negligible nonlinear refraction effects compared to the HSG-composites at the same excitation laser power regime. A notable feature detected in the NLO experiments performed in these hybrid composites is the large asymmetry observed in their respective Z-Scan transmittance curves; this phenomenon may arise either from NLO-absorption or laser-induced thermal effects, which might become important due to the cw-laser excitation mode implemented during long/slow Z-Scan measurements (although our experimental conditions were far from the resonance regime).

In order to perform the theoretical fits (TFs), the normalized Z-Scan transmittance T_N can be determined as a function of the dimensionless sample position ($x = z/z_0$), where z_0 is the Rayleigh range and z is the actual Z-Scan sample position. Hence, the TFs (for samples A–B) were obtained according to the following relation (Liu et al., 2001):

$$T_N \approx 1 + \left[\frac{4x}{(1+x^2)(9+x^2)}\right]\Delta\Phi - \left[\frac{2(x^2+3)}{(1+x^2)(9+x^2)}\right]\Delta\Psi$$

Here, the first term corresponds to a normalizing constant. The second term is related to NLO-refractive effects, whereas the third one is associated to NLO-absorptive phenomena. Indeed, since the obtained Z-Scan data exhibit important valley-to-peak transmittance asymmetries, NLO absorptive effects are expected (Liu et al., 2001). The fitting parameters are in this case the induced phase shifts $\Delta\Phi$ or $\Delta\Psi$, respectively. In the former case, the phase shift is given by $\Delta\Phi = 2\pi\gamma I_0 L_{eff}/\lambda$, from which the NLO refractive index (γ-coefficient) can be obtained. In the latter case, the phase shift is provoked by the NLO-absorption of the sample and is given by $\Delta\Psi = \beta I_0 L_{eff}/2$, allowing the evaluation of the NLO-absorption (β-coefficient) either due to multi-photon absorption ($\beta > 0$) and/or to saturable absorption effects ($\beta < 0$). In these equations, λ is the laser wavelength, I_0 is the input beam intensity (at focal spot: $z = 0$) and L_{eff} is the effective thickness of the sample, defined as $L_{eff} = [1 - (e^{-\alpha_0 L_s})](\alpha_0)^{-1}$, where α_0 represents the linear absorption coefficient. In most cases (mainly in the case of well-defined $\gamma > 0$ or $\gamma < 0$ curves); our experimental results nearly satisfy the theoretical restrictions imposed by these formulas and can be conveniently fitted according to these theoretical approximations. Thus, for comparison purposes and in order to be consistent with the estimation of the γ- and β-values, we have assumed their applicability and use to fit our experimental data. Hence, the TFs allowed us to evaluate a huge positive NLO γ-refractive coefficients for the CdTe-QDs/SiO_2 HSG samples in the promising order of $10^{-8}\,m^2\,W^{-1}$ (HSG-A: $\gamma = +14.6 \times 10^{-8}\,m^2\,W^{-1}$, HSG-B: $\gamma = +8.8 \times 10^{-8}\,m^2\,W^{-1}$). The obtained γ-values of our samples are many orders of magnitude larger than those observed for typical glass substrates or the classical CS_2 reference material (Sheik-Bahae et al., 1989, 1990). The magnitude dependence of the NLO γ-refractive coefficients with the QDs size can be attributed to variations on the crystallinity of the samples and to quantum confinement effects which clearly depend on the size of the CdTe-crystals. On the other hand, the marked asymmetries observed in the Z-Scan curves can be attributed to a counterbalancing response provoked by NLO-absorptive effects (Liu et al., 2001). Indeed, a complex light-matter interaction and a strong influence of the CdTe-QDs structures within the sonogel matrix lead to the observation of NLO absorption mechanisms. According to the experimental data and the corresponding TFs shown in Figure 6, the sign of the β-coefficients and the nature of the NLO absorptive phenomena occurring within our hybrid samples are revealed. Results indicate strong NLO absorptive phenomena due to saturable absorption effects (SA, $\beta < 0$, in the order of $10^{-1}\,m\,W^{-1}$) for both CdTe-QDs/SiO_2 HSG samples (HSG-A: $\beta_{SA} = -6.2 \times 10^{-1}\,m\,W^{-1}$, HSG-B: $\beta_{SA} = -9.3 \times 10^{-1}\,m\,W^{-1}$). These results indicate convenient material properties to avoid undesired photo-thermal effects during long Z-Scan experiments under cw-laser irradiation. In any case, it is then clear that further Z-Scan experiments (in open- and closed-aperture modes and at different wavelengths) will be required in order to further understand the NLO-absorptive/refractive properties of these interesting nanostructured hybrid materials. This will allow us for instance, to elucidate the influence of the free-electron activity, intra- and/or inter-band electronic transitions of the confined CdTe-QDs.

4. Conclusions

In this work the synthesis of CdTe nanocrystals in aqueous solution (Cd/Te 4:1, 2–3 μm in diameter) and the preparation of CdTe-QDs/SiO_2-based HSG-composites at different dopant concentrations were successfully reported. The CdTe-QDs systems were homogeneously dispersed within the dielectric sonogel networks in order to obtain stable guest-host nanostructured composites suitable for linear and nonlinear photophysical investigations. The mesoporous properties obtained at room temperature processing from the sonogel glasses, together with their stable mechanical performance, provided an excellent environment for the solid-state confinement of CdTe-QDs in rigid/bulky composites. This suggests the development of new functionalized inorganic–inorganic optical materials whereby controllable low/high doping rates can be supported. These composites can be produced at relatively low cost and elevated mechanical/optical control with the advantage that the QDs-aggregation can be notably inhibited. Thus, the optical properties of the QDs-NCs can be studied in a quasi-pristine state. In fact, Raman spectroscopy studies have shown that CdTe-QDs can be supported within the densely packed SG-environment preserving their low dimensional properties (as QDs or probably as tetrapod NC-structures). On the other hand, PL-measurements exhibited the possibility of obtaining strong PL-intensities from the HSG-glasses with direct applications in blue-ray laser materials and other opto-electronic devices requiring narrow bandwidth emissions. Finally, the cubic NLO-activity of the developed hybrid films was tested via Z-Scan measurements. Experimental results indicate that the confined

CdTe-QDs samples exhibit large positive NLO-refractive properties and saturable absorptive NLO-effects. However, our results point to a complex dependence of the NLO-properties of these HSG-systems on the quantum confinement effects and on the crystallite properties of the CdTe-QDs. All these facts suggest a complex light-matter interaction occurring in our HSG-glasses and additional Z-Scan and XRD spectroscopic investigations should be performed in order to further understand the photophysical and electronic characteristics of the CdTe-QDs within the sonogel confinement. These studies are currently underway and will be presented in detail in a future work, including resonant and non-resonant Z-Scan measurements.

Conflict of interest

The authors have no conflicts of interest to declare.

Acknowledgments

We are grateful to Dra. María Esther Mata-Zamora (CCADET-UNAM) for her valuable support on Raman spectroscopic measurements. O.G.M.S. acknowledges financial support from the DGAPA/PAPIIT/UNAM-IG100713 project grant.

References

Ando, M., Hosokawa, C., Yang, P., & Murase, N. (2012). Electroluminescence of hybrid self-organised fibres incorporating CdTe quantum dots. *Australian Journal of Chemistry*, *65*(9), 1257–1259.

Brus, L. E. (1984). Electron–electron and electron–hole interactions in small semiconductor crystallites: The size dependence of the lowest excited electronic state. *The Journal of Chemical Physics*, *80*(9), 4403–4409.

Chao, M. R., Hu, C. W., & Chen, J. L. (2014). Comparative syntheses of tetracycline-imprinted polymeric silicate and acrylate on CdTe quantum dots as fluorescent sensors. *Biosensors and Bioelectronics*, *61*, 471–477.

Chen, J., Chen, X., Xu, R., Zhu, Y., Shi, Y., & Zhu, X. (2008). Refractive index of aqueous solution of CdTe quantum dots. *Optics Communication*, *281*(13), 3578–3580.

Chu, M., Pan, X., Zhang, D., Wu, Q., Peng, J., & Hai, W. (2012). The therapeutic efficacy of CdTe and CdSe quantum dots for photothermal cancer therapy. *Biomaterials*, *33*(29), 7071–7083.

De Paula, A. M., Barbosa, L. C., Cruz, C. B., Alves, O. L., Sanjurjo, J. A., & Cesar, C. L. (1996). Size effects on the phonon spectra of quantum dots in CdTe-doped glasses. *Applied Physics Letters*, *69*(3), 357–359.

Eugene, H. (2002). *Optics* (3rd ed.). Reading, MA, USA: Addison Wesley.

Flores-Flores, J., & Saniger, J. M. (2006). Catalyst-free SiO_2 sonogels. *Journal of Sol–Gel Science and Technology*, *39*(3), 235–240.

Gao, M., Lesser, C., Kirstein, S., Möhwald, H., Rogach, A. L., & Weller, H. (2000). Electroluminescence of different colors from polycation/CdTe nanocrystal self-assembled films. *Journal of Applied Physics*, *87*(5), 2297–2302.

Gao, X., Cui, Y., Levenson, R. M., Chung, L. W., & Nie, S. (2004). In vivo cancer targeting and imaging with semiconductor quantum dots. *Nature Biotechnology*, *22*(8), 969–976.

Gaponik, N., Talapin, D. V., Rogach, A. L., Hoppe, K., Shevchenko, E. V., Kornowski, A., et al. (2002a). Thiol-capping of CdTe nanocrystals: An alternative to organometallic synthetic routes. *Journal of Physical Chemistry B*, *106*(29), 7177–7185.

Gaponik, N., Talapin, D. V., Rogach, A. L., Eychmüller, A., & Weller, H. (2002b). Efficient phase transfer of luminescent thiol-capped nanocrystals: From water to nonpolar organic solvents. *Nano Letters*, *2*(8), 803–806.

Gu, Z., Zou, L., Fang, Z., Zhu, W., & Zhong, X. (2008). One-pot synthesis of highly luminescent CdTe/CdS core/shell nanocrystals in aqueous phase. *Nanotechnology*, *19*(13), 135604.

Gutiérrez-Lazos, C. D., Ortega-López, M., Rosendo-Andrés, E., Matsumoto-Kuwabara, Y., Sánchez-Reséndiz, V., Morales-Corona, J., et al. (2010). pp. 374–379. *Highly luminescent CdTe nanocrystals synthesized in aqueous solution and self-assembled on polyelectrolyte multilayers* (Vol. 636–637) Switzerland: Materials Science Forum/Trans. Tech. Publications Ltd. http://dx.doi.org/10.4028/www.scientific.net/MSF.636-637.374

Harrison, M. T., Kershaw, S. V., Burt, M. G., Rogach, A. L., Kornowski, A., Eychmüller, A., et al. (2000). Colloidal nanocrystals for telecommunications. Complete coverage of the low-loss fiber windows by mercury telluride quantum dot. *Pure and Applied Chemistry*, *72*(1–2), 295–307.

Hollingsworth, J. A., Mikhailovsky, A. A., Malko, A., Klimov, V. I., Leatherdale, C. A., Eisler, H. J., et al. (2001). Nanocrystal quantum dots: Building blocks for tunable optical amplifiers and lasers. *MRS-Proceedings*, *667* http://dx.doi.org/10.1557/PROC-667-G6.1. G6.1

Huang, W. J., De Valle, S. A., Kana, J. B. K., Simmons-Potter, K., & Potter, B. G. (2015). Integration of CdTe–ZnO nanocomposite thin films into photovoltaic devices. *Solar Energy Materials and Solar Cells*, *137*, 86–92.

Kagan, C. R., Murray, C. B., & Bawendi, M. G. (1996). Long-range resonance transfer of electronic excitations in close-packed CdSe quantum-dot solids. *Physical Review B*, *54*, 8633–8643.

Kostić, R., & Stojanović, D. (2012). Electric field effect on the nonlinear and linear intersubband absorption spectra in CdTe/ZnTe spherical quantum dot. *Journal of Nanophotonics*, *6*(1), 061606–61611.

Li, D., Liu, X., Xie, G., & Liu, X. (2013). Stable and water-soluble CdTe@ SiO_2 composite nanospheres: Preparation, characterization and application in LED. *Colloids and Surfaces A: Physicochemical and Engineering Aspects*, *424*, 33–39.

Liu, X., Guo, S., Wang, H., & Hou, L. (2001). Theoretical study on the closed-aperture Z-scan curves in the materials with nonlinear refraction and strong nonlinear absorption. *Optics Communication*, *197*(4–6), 431–437.

Morales-Saavedra, O. G., Rivera, E., Flores-Flores, J. O., Castañeda, R., Bañuelos, J. G., & Saniger, J. M. (2007). Preparation and optical characterization of catalyst free SiO_2 sonogel hybrid materials. *Journal of Sol–Gel Science and Technology*, *41*(3), 277–289.

Morales-Saavedra, O. G., Zanella, R., Maturano-Rojas, V., Torres-Zúñiga, V., Flores-Flores, J. O., Rodríguez-Rosales, A. A., et al. (2012). Preparation and Z-Scan nonlinear optical characterization of Au/SiO_2-and Ag/SiO_2-supported nanoparticles dispersed in silica sonogel films. *Journal of Sol–Gel Science and Technology*, *63*(3), 340–355.

Murray, C., Norris, D. J., & Bawendi, M. G. (1993). Synthesis and characterization of nearly monodisperse CdE (E = sulfur, selenium, tellurium) semiconductor nanocrystallites. *Journal of the American Chemical Society*, *115*(19), 8706–8715.

Rajbanshi, B., Sarkar, S., & Sarkar, P. (2014). Band gap engineering of graphene–CdTe quantum dot hybrid nanostructures. *Journal of Materials Chemistry C*, *2*(42), 8967–8975.

Rodríguez-Rosales, A. A., Morales-Saavedra, O. G., Román-Moreno, C. J., & Ortega-Martínez, R. (2008). Variation of nonlinear refractive index in dye-doped liquid crystals by local and nonlocal mechanisms. *Optical Materials*, *31*(2), 350–360.

Rogach, A. L., Franzl, T., Klar, T. A., Feldmann, J., Gaponik, N., Lesnyak, V., et al. (2007). Aqueous synthesis of thiol-capped CdTe nanocrystals: State-of-the-art. *Journal of Physical Chemistry C*, *111*(40), 14628–14637.

Schlamp, M. C., Peng, X., & Alivisatos, A. P. (1997). Improved efficiencies in light emitting diodes made with CdSe (CdS) core/shell type nanocrystals and a semiconducting polymer. *Journal of Applied Physics*, *82*(11), 5837–5842.

Sehgal, P., & Narula, A. K. (2015). Synthesis and characterization of quantum dot sensitized solar cell based on PMOT@ CdTe@ TiO_2 core–shell nanostructures. *Electrochimica Acta*, *158*, 49–55.

Sheik-Bahae, M., Said, A. A., & Van Stryland, E. W. (1989). High-sensitivity, single-beam n2 measurements. *Optics Letters*, *14*(17), 955–957.

Sheik-Bahae, M., Said, A., Wei, T. H., Hagan, D. J., & Van Stryland, E. W. (1990). Sensitive measurement of optical nonlinearities using a single beam. *IEEE Journal of Quantum Electronics*, *26*(4), 760–769.

Talapin, D. V., Rogach, A. L., Kornowski, A., Haase, M., & Weller, H. (2001). Highly luminescent monodisperse CdSe and CdSe/ZnS nanocrystals synthesized in a hexadecylamine-trioctylphosphine oxide-trioctylphospine mixture. *Nano Letters*, *1*(4), 207–211.

Torres-Zúñiga, V., & Morales-Saavedra, O. G. (2012). Structural and nonlinear optical properties of Crystal-Violet octupolar dyes dispersed in bulk SiO_2-sonogel optical-glasses. *Materials Chemistry and Physics*, *133*(2), 1071–1082.

Tu, M. L., Su, Y. K., & Chen, R. T. (2014). Hybrid light-emitting diodes from anthracene-contained polymer and CdSe/ZnS core/shell quantum dots. *Nanoscale Research Letters*, *9*(1), 1–5.

Zhao, D., Sun, L., Wang, Y., Du, Y., & Wang, C. (2012). Preparation and application of CdTe nanocrystals. *Progress in Chemistry*, *24*(7), 1277–1293.